Journal of Ultrafine Grained and Nanostructured Materials
https://jufgnsm.ut.ac.ir
Vol. 54, No.1, June 2021, pp. 1-20
Print ISSN: 2423-6845 Online ISSN: 2423-6837
DOI: 10.22059/jufgnsm.2021.01.01

Friction stir welding of ultrafine grained aluminum alloys: a review

M. Sarkari Khorrami

School of Metallurgy and Materials Engineering, College of Engineering, University of Tehran, Tehran, Iran.

Recieved: 10 April 2021; Accepted: 25 April 2021
** Corresponding author email: m.khorrami@ut.ac.ir*

ABSTRACT

Severe plastic deformation (SPD) has been one of promising routes to fabricate ultrafine-grained (UFG) materials, especially aluminum alloys. However, the SPD products often suffer from their small size. This issue implies the necessity of welding of UFG aluminum alloys for making them usable in complex, large forms in industries. Among various welding processes, those based on solid state welding seem to be more consistent with UFG materials. This is associated with the instability of UFG materials upon intense heating cycle that is common in fusion state welding processes. Friction stir welding (FSW) as a well-known process in the category of solid state welding is widely used for welding of aluminum alloys. This review paper provides an overview of the state-of-the-art of FSW of UFG aluminum alloys. To do so, specific attention is given to microstructural and textural evolutions, effect of secondary particles, and cooling medium. Applying cryogenic cooling medium as well as secondary nanoparticles could inhibit excessive grain growth in the stir zone, which were beneficial to improve the strength of the stir zone without remarkable decrease in the ductility. These processing routes did not affect the main recrystallization mechanism of the stir zone.

Keywords: *Ultrafine grained aluminum; Friction stir welding; Severe plastic deformation; Microstructure; Texture; Electron Backscattered diffraction.*

1. Introduction

Ultrafine grained (UFG) metals, specifically aluminum alloys, have attracted growing attention due to superior mechanical properties that could be obtained. One of the most effective route to fabricate UFG metals is based on severe plastic deformation (SPD) [1] in which grain subdivision progressively occurs during various stages of deformation [2]. Many diverse SPD methods have been developed for metals in the form of sheet [3,4] and even tube [5]. In spite of existence of different SPD routes, they all have similar drawbacks. As the extent of applying force and the dimension of dies used in SPD are restricted, the size of severely plastic deformed products is often small confining their applicability in industries [6,7]. Therefore, the welding of such kind of materials is of significant matter. The UFG structure usually contains unstable grain boundaries making them susceptible to heating cycle, so that recrystallization and fast grain growth possibly take place [8]. Thus, fusion welding processes are not suitable candidate for this purpose as they impose high magnitude of heat to the base metal [6]. Also, the cast microstructure is obtained in the weld zone deteriorating mechanical properties of the joint. This issue implies the use of solid state welding processes for UFG metals [9], among which friction stir welding (FSW) is more interesting [10]. Although the amount of heat in FSW is quite lower than that of fusion welding processes, UFG metals would experience grain growth during FSW likewise [11]. In fact, the stored strain in the base metal has

considerable influences on the evolution of grain structure in the weld zone of FSW joints [12].

There are many review papers in the literature regarding SPD [13,14], nanostructured or UFG materials [15,16], and FSW [17]; however, the FSW of UFG aluminum alloys has not comprehensively been reviewed. The present paper gives a brief description on SPD and FSW in sections 2 and 3. Then, a detailed evaluation of a number of research studies on the FSW of UFG aluminum is reviewed in section 4 with focusing on the microstructural and textural evolutions. This is followed by the effect of secondary particles and cooling media.

2. Brief review of SPD

Over the past decade, tremendous researches have been carried out in the field of nanocrystalline and UFG materials with a grain size lower than 100 nm [1] and 1 μm [18], respectively. These materials could be achieved by introducing a high fraction of grain boundaries, which is responsible for their unusual properties such as high mechanical strength and toughness [19]. There are two basic routes to fabricate nanocrystalline materials, namely bottom-up and top-down. The methods based on bottom-up techniques usually have important drawbacks, i.e. the limited product size and high residual porosity in products fabricated by consolidation of nanopowders [20]. The other approach (top-down techniques) is based on SPD in which a metal is heavily strained under high pressure leading to the formation of bulk nanocrystalline metals without any considerable change in its overall dimensions [21]. Copious methods have been developed in the field of SPD to fabricate UFG metals some of which are equal-channel angular pressing (ECAP) [22], accumulative roll bonding (ARB) [4,23], constrained groove pressing (CGP) [3] high-pressure torsion (HPT) [24,25], and multi-axial incremental forging and shearing (MAIFS) [26]. Grain refinement mechanism in SPD includes progressive grain-subdivision through imposing strain. At earlier stage of straining, the dislocation density increases. Then, dislocation rearrangement occurs causing subgrain structure to form. Applying more strain changes low-angle grain boundaries (LAGBs) to high-angle grain boundaries (HAGBs) [27]. The presence of 70-80% of HAGBs in metals processed by multipass SPD is of common microstructural observation [28]. Shin et al. [3] reported on the grain refinement of aluminum from ~1.2 mm in the annealed state to around 0.8 μm after four passes of CGP. Also, a nano-sized crystallite size (~103 nm) was reported for a pure aluminum after 10 cycles of circular simple shear extrusion process [29]. Mechanical properties of a metal processed by a SPD route vary considerably with the SPD passes since the structure of grain boundaries depends on the magnitude of imposed strain [1]. Most researchers unanimously believe that mechanical strength of a metal significantly increases during the initial stage of SPD (i.e. the first pass) and further deformations make minor improvement in mechanical properties. For example, Huang et al. [30] examining the effect of ECAP pass numbers on the mechanical properties of a high-calcium-content Mg-Al-Ca-Mn alloy reported of minor discrepancy in strength of specimens processed by 4 and 8 passes of ECAP. Also, Zrnik et al. [31] studied microstructure evolutions and deformation behavior of aluminum during the CGP process. In accordance with their results, the main improvement in strength was achieved after one pass while the strength reached a maximum after four passes.

3. Brief overview of FSW

The FSW process emerges as the most popular solid state welding process that invented by The Welding Institute of UK in 1991 [17]. This process was initially utilized for welding of aluminum alloys that known as hard-to-weld alloys [32]. In FSW, a non-consumable rotating tool with a particularly designed shoulder and pin is plunged into a specific area between two workpieces [33]. Localized frictional heat as well as the plastic deformation of the workpieces softens the material beneath the FSW tool. The combined rotational and traveling movements of the tool cause the softened material to flow from the front of the tool to its back completing a joint in the solid state [17]. Thus, FSW possesses lower welding heat input in comparison with fusion state welding processes making it suited for the welding of UFG materials [6]. In recent decades, friction stir processing (FSP) has received great attention in surface engineering. This process is also beneficial to modify the microstructure of cast alloys in terms of uniformly dispersed secondary phases [34]. This process is principally based on FSW without the aim of joining. When a rotating tool comes in contact with the surface of an alloy, the material beneath the tool experiences SPD at elevated temperature, namely hot deformation [35]. So, dynamic recovery (DRV) [36] or dynamic recrystallization (DRX) [37,38] phenomena

would govern the microstructure evolutions in the deformed, or stir zone. It has been found that FSP has potential to produce a bulk UFG aluminum alloy with grain size of 100-400 nm by running overlapped passes followed by rapid cooling [39]. Also, Su et al. [40] reported of an UFG microstructure with an average grain size of 174 nm in stir zone of copper after FSP conducted with continuous cooling.

4. FSW/FSP of severely deformed Al alloys

SPD products generally suffer from small product size in spite of their copious advantages. This is mainly caused by restricted applying load, dimensions of dies, and rigidity of equipment. Moreover, the geometry of metals undergone SPD is often limited to routine shapes. These issues signify the necessity of welding of SPD products for possible industrial use [41]. However, grain boundaries in severely deformed metals are not in equilibrium condition due to the presence of excessive dislocations, which do not have great contribution in increasing misorientation between grains [31]. These non-equilibrium grain boundaries make SPD products susceptible to any subsequent heating or thermomechanical process [42-45]. Thus, grain coarsening is of common observation not only in the stir zone but also in heat affected zone (HAZ) and thermomechanical affected zone (TMAZ) [46]. The welding of severely deformed alloys with UFG microstructure is likewise confronted with great challenges. Innovative processing routes have been developed to overcome these difficulties which are reviewed in the present paper.

4.1. Microstructure evolutions and texture variations

Various mechanisms have been reported for evolution of stir zone microstructure during FSP of aluminum alloys. Fonda et al. [36] declared that deformation-induced grain subdivision followed by DRV was responsible for formation of equiaxed grains in the stir zone of 2195 aluminum alloy. They did not observe any evidence of DRX. On the other hand, Prangnell et al. [37] and Su et al. [47,48] reported of combined DRV and other recrystallization phenomena controlling microstructure of stir zone in aluminum alloys. Jata et al. [49] and Kumar et al. [50] argued that continuous DRX (CDRX) or discontinuous DRX (DDRX) mechanism is primarily pronounced in the formation of equiaxed grains in the stir zone in spite of high stacking fault energy of aluminum alloys. However, some researchers believe that DDRX would be retarded during FSW of aluminum alloys as their high stacking fault energy facilitates cross-slip and dislocation climb suppressing accumulation of strain needed for nucleation of new grains [48]. So, the mechanism of microstructure development during FSW/FSP of aluminum alloys remains still unclear. This situation becomes even more complicated in the case of FSW/FSP of severely deformed aluminum since the strain stored in the

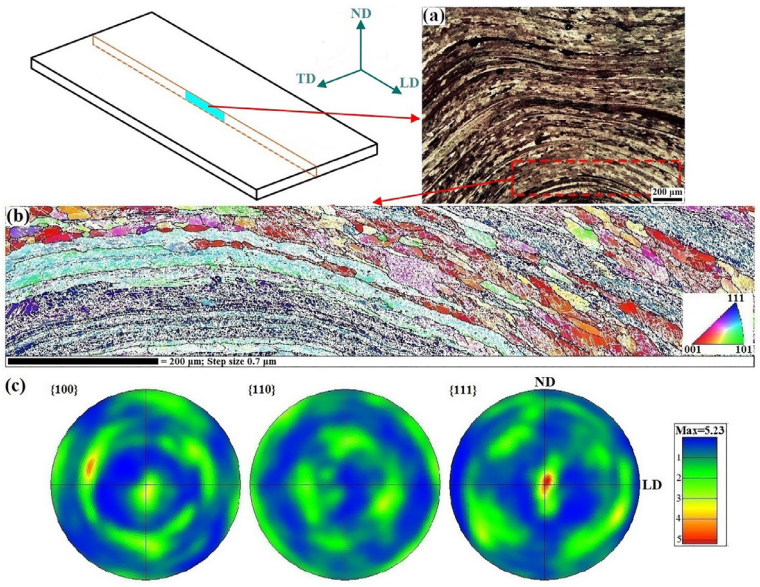

Fig. 1- (a) Optical microscopy image, (b) inverse pole figure map, and (c) pole figures at the longitudinal section of 1050 aluminum alloy severely deformed through 2 passes of CGP [54].

base metal affects microstructure evolutions during subsequent thermomechanical process [51]. In order to apprehend this effect, Khorrami et al. [52] studied microstructure and texture developments during FSP of 1050-aluminum alloy, which was severely deformed through 2 passes of CGP process. This examination included electron backscattered diffraction (EBSD) analysis from a longitudinal section covering areas located ahead and beneath the FSP tool. The microstructure located quite far from the position of the FSP tool (corresponding to the base metal) is indicated in Fig. 1. As shown, elongated grains (dark boundaries) with the corrugated pattern and interior substructure (white boundaries) with a preferential grain orientation were formed in the alloy after the CGP process. Orientation distribution function (ODF) maps from this section (Fig. 2) manifested the development of $\{1\bar{1}2\}\langle 110\rangle/\{\bar{1}1\bar{2}\}\langle\bar{1}\bar{1}0\rangle$ (corresponding to $B/\bar{B}$ ideal shear texture component), $\{011\}\langle 011\rangle$ rotated Goss, $\{110\}\langle\bar{1}12\rangle$ Brass, and $\langle 100\rangle\|ND$ (θ-fiber) texture components. Rotated Goss and Brass texture components were also observed in the aluminum alloy after ARB process [53].

During FSP of UFG alloy, the tool was stopped at the middle of the path. Fig. 3 (a) shows inverse pole figure map from front regions of the FSP tool. It can be seen that the elongated grains were replaced by equiaxed, large grains with almost random orientation (Fig. 3 (b)). The combined effects associated with the prestraining caused by CGP and temperature rise by FSP led to the incident of static recovery, recrystallization, and grain growth ahead of the tool before being stirred by the rotating tool. This phenomena deteriorated UFG structure preliminarily formed in the base metal. In the vicinity of the FSP tool, grains were elongated along dotted line mainly due to the deformation field applied by the tool. An increase in the fraction of LAGBs (white lines) had a sign of initiation of DRV. Moreover, the deformation field resulted in the preferential grain orientation, e.g. the $\langle 110\rangle$ direction was aligned near the tool movement direction (TMD) corresponding to B-fiber shear texture (see Fig. 3 (c)) [52].

Fig. 4 shows the inverse pole figure map and pole figures from beneath the tool (stir zone). The elongated grains in the deformation field were

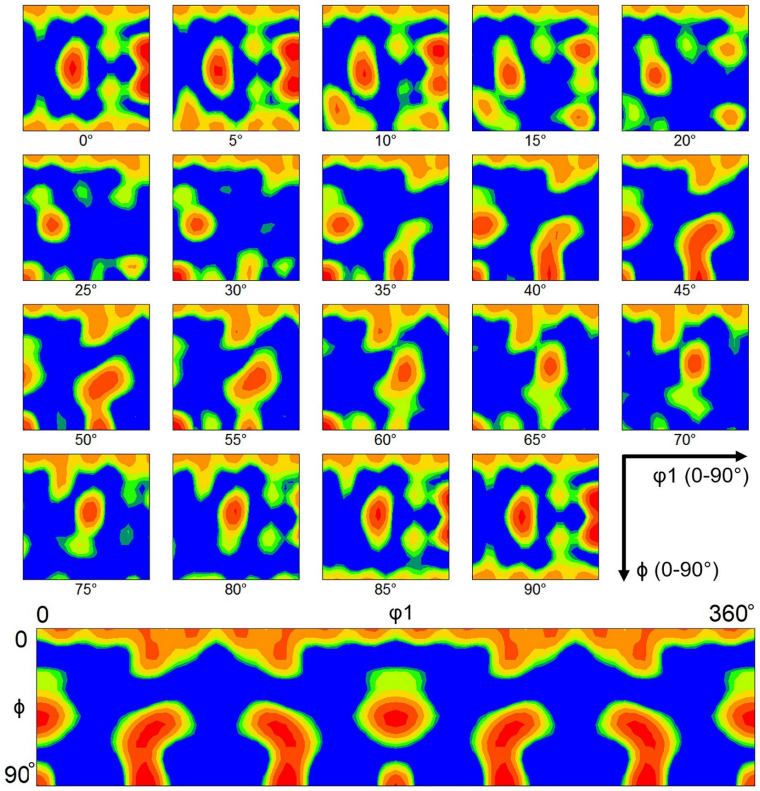

Fig. 2-ODF maps for 1050 Al alloy undergone 2 passes of CGP at the Euler space angles of ϕ1=0–90° and φ=0–90° at ϕ2 sections in 5° intervals (top) and at the Euler space angles of ϕ1=0–360° and φ=0–90° at section ϕ2=0 (bottom) [54].

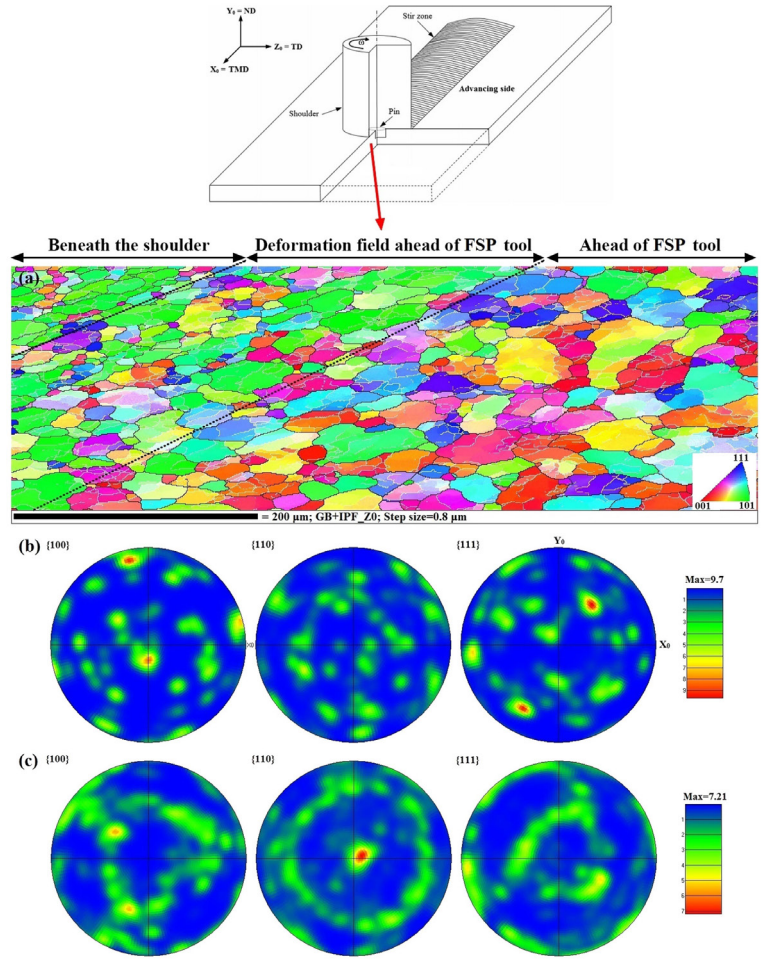

Fig. 3- (a) Inverse pole figure map indicating the microstructure evolutions from regions ahead of the FSP tool to regions beneath the shoulder, (b) and (c) pole figures from ahead of the tool and deformation field, respectively [52].

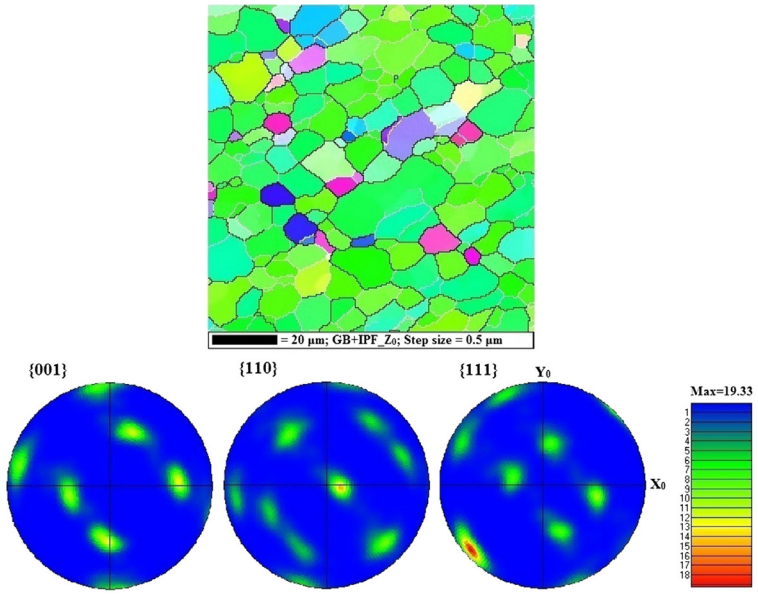

Fig. 4- Inverse pole figure map and pole figures from the stir zone of 1050 aluminum alloy processed by CGP and subsequent FSP [52].

replaced by the equiaxed, fine grains, suggesting the incident of DRX. However, the grain orientation was similar to that observed in the deformation field. The strength of shear texture components (C and A_1^*) became stronger signifying the completion of shear texture development. Simple shear texture development was also observed in duplex stainless steel after FSP [55]. The replacement of elongated grains with equiaxed ones without any change in textural characteristics was the sign of geometrical DRX (GDRX) [52]. Comparing the stir zone microstructures of the severely deformed aluminum and the annealed counterpart, it can be found that microstructure instability ahead of the tool during FSP affects final microstructure in the stir zone. This results in the formation of coarser grain size in the stir zone of the severely deformed aluminum [51].

Sun et al. [6] studied microstructure evolutions of 1050 aluminum alloy in accumulative roll bonded (ARBed), ARBed followed by H24 annealing, and as-received conditions during FSW. As can be seen from EBSD maps of the above specimens (Fig. 5), three different grain sizes were obtained. The equivalent stir zone microstructures are shown in Fig. 6. The stir zone of ARBed specimen exhibited the largest grain size although it had the smallest grain size before FSW compared to the as-received and ARBed + H24 annealing counterparts. Accordingly, the ARBed specimen was quite unstable upon subsequent heating/thermomechanical process in which rapid grain growth was pronounced rather than the fragmentation of UFG microstructure by shear stress induced by the rotating tool. The same results were reported by Sun et al. [56] studying dissimilar

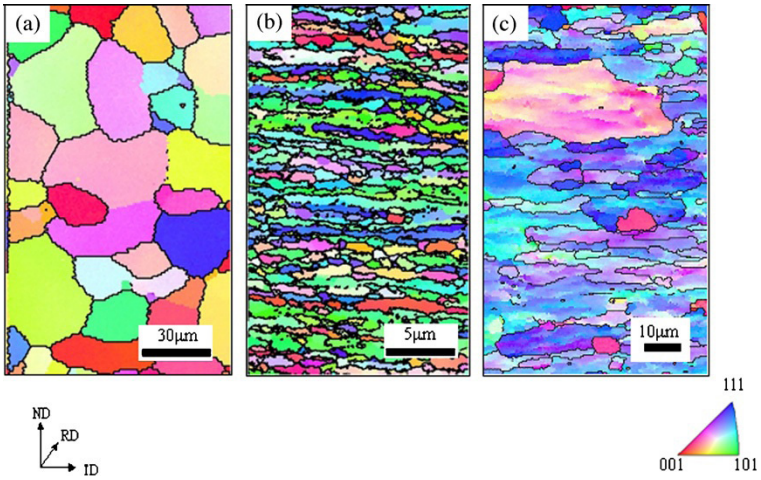

Fig. 5- EBSD maps of (a) as-received, (b) ARBed, and (c) ARBed followed by H24 annealing [6].

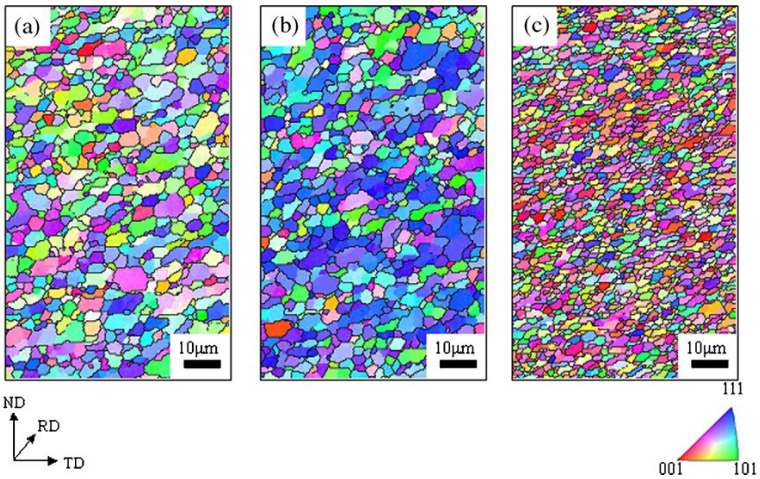

Fig. 6- EBSD maps from the stir zone of specimens in the (a) as-received, (b) ARBed, and (c) ARBed followed by H24 annealing conditions; rotational and translate speeds are 1000 rpm and 1000 mm.min^{-1}, respectively [6].

FSW of UFG 1050 to 6061-T6 aluminum alloys. The UFG 1050 alloy exhibited instability during FSW in terms of recrystallization and subsequent grain growth while grain refinement occurred in 6061-T6 alloy.

Bead on plate FSW, or FSP, of ARBed aluminum alloys was also characterized by Sato et al. [12]. Fig. 7 (a) indicates transmission electron microscopy (TEM) images of an 1100 aluminum alloy processed by 6 cycles of ARB process. The microstructure consisted of pancake-shaped ultrafine grains (with width and length of 260 and 450 nm, respectively) surrounded by HAGBs. Moreover, dislocations and substructure existed interior the elongated grains. Referring to Fig. 7 (b), the stir zone included mainly equiaxed grains with an average size of 870 nm as a result of DRX. The grain size of stir zone was coarser than that of the base metal probably due to the grain growth induced by frictional heat generated in the stir zone. It was also declared that the ARBed material just outside of the stir zone experienced small grain growth and recovery of dislocations that made FSW process suited for the welding of UFG metals.

Topic et al. [10] examined FSW of 1050 (in the cold rolled condition) and 6016 (in T4 state) aluminum alloys after ARB process. Their results showed that reduction in dislocation density as well as grain coarsening took place in the stir zone, namely from 200 nm in the ARBed condition to around 1 μm in the stir zone. Based on the same hardness values of the stir zone of ARBed and coarse grained base metals, they concluded that prestraining of the base metal has no effect on the final microstructure of the stir zone. This argument is entirely in contrast to those reported in [6,51].

4.2. Effect of secondary nanoparticles

Microstructure instability of UFG aluminum alloys during FSW/FSP as a result of their tendency for grain boundary migration causes coarse grains to form in the stir zone. Several studies have been carried out so far to investigate the possibility of grain boundary pinning through applying secondary particles during FSP of UFG aluminum alloy [57,58]. Material flow at elevated temperature enables FSP to distribute secondary particles in an aluminum matrix leading to the fabrication of surface composites or nanocomposites [59-62]. The application of secondary particles could effectively improve mechanical properties and wear behavior of a metallic matrix if they are properly dispersed [63]. There are some important parameters in FSP that significantly affect material flow and then distribution of secondary particles in the stir zone. The most determinant factors are

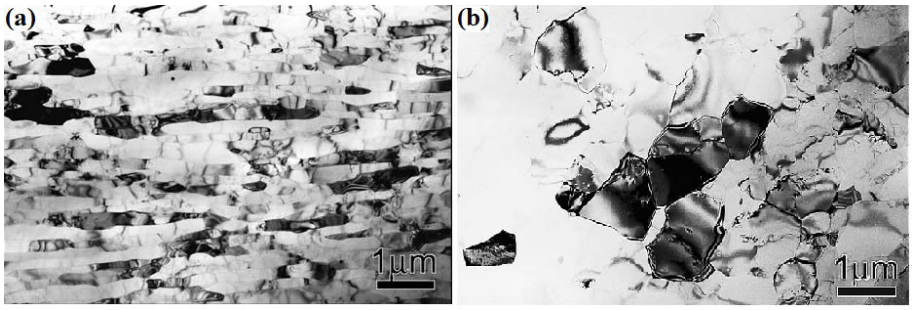

Fig. 7- TEM images showing microstructure of (a) ARBed specimen and (b) stir zone after FSW process [12].

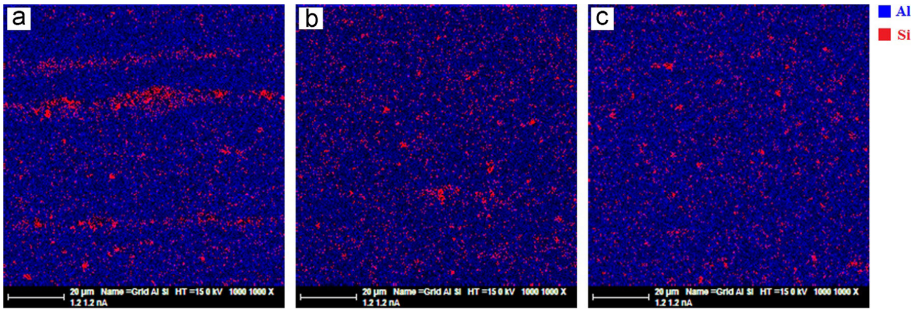

Fig. 8- Elemental maps of aluminum and silicon achieved from energy dispersive spectroscopy (EDS) showing distribution of SiC nanoparticles in the stir zone after (a) 1, (b) 2, and (c) 3 FSP passes [58].

FSP pass numbers [58] as well as the geometry of the FSP tool [64]. Notably, this processing route has positive effects only on the stir zone. Thus, in the case of FSP of UFG aluminum alloy, it is quite critical to obtain well-dispersed particles with the least FSP passes (and then the lowest heat input) because of softening in HAZ. A research study on the FSP of severely deformed aluminum using SiC nanoparticles [58] revealed that large clusters of nanoparticles were formed at the retreating side of the stir zone when 1 or 2 passes of FSP were applied. However, the third FSP pass resulted in the fairly uniform distribution of nanoparticles (Fig. 8). The existence of clusters created weak interface with the aluminum matrix acting as stress concentration sources during tensile test. It suggested initiation of brittle fracture from the interface of the clusters and the matrix. The observation of secondary particles at the fracture surface confirmed this issue. In case of uniform distribution of nanoparticles, the stir zone exhibited acceptable mechanical properties in such a way that fracture occurred outward from the stir zone.

In another study [57], it has been reported that a change in the rotational direction of the FSP tool between passes as well as using a threaded pin could effectively improve the distribution of nanoparticles in the stir zone even after 2 passes of FSP. In fact, these factors could effectively break the cluster of nanoparticles. The achievement of uniform distribution of nanoparticles at lower FSP passes could increase the strength of processed specimens during transverse tensile test due to the less softening in HAZ. The influence of volume fraction of secondary nanoparticles during FSP of 1050 aluminum alloy severely deformed by 2 passes of CGP process was investigated by Khorrami et al. [65]. They found that the application of FSP without nanoparticles deteriorated the subgrain structure preliminarily formed during CGP process and increased the grain size to ~10 μm in the stir zone. A significant reduction in the fraction of LAGBs was also evident. Texture variations occurred likewise so that $\{001\}\langle 100\rangle$ Cube, $\{011\}\langle 011\rangle$ rotated Goss, $\{110\}\langle \bar{1}12\rangle$ Brass, and $\{\bar{1}1\bar{2}\}\langle \bar{1}\bar{1}0\rangle$ $B/\bar{B}$ shear components developed in the aluminum alloy processed by CGP were replaced by $\{001\}\langle 110\rangle$ rotated Cube and ideal shear component C after FSP without secondary particles (see Fig. 9). When 1.5 volume percent of SiC was applied during

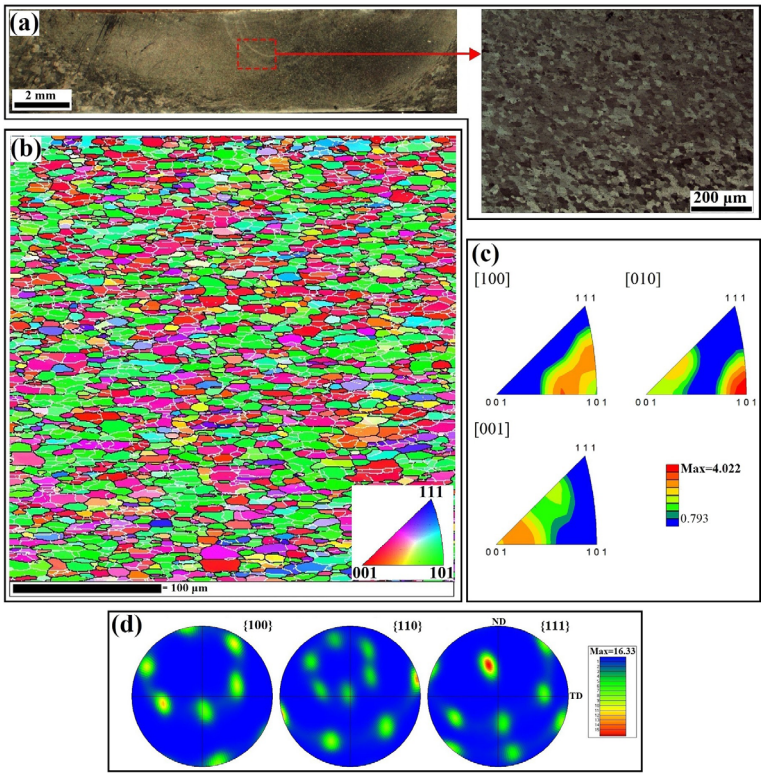

Fig. 9- Experimental results of 1050 aluminum alloy processed by 2 passes of CGP and subsequent 1 pass of FSP without secondary particles: (a) optical macro- and micrograph, (b) EBSD grain orientation map, (c) inverse pole figures, and (d) pole figures from the stir zone [65].

FSP, the stir zone grain size decreased to ~5.6 μm. This was mainly attributed to the pinning effect of nanoparticles that restricted grain boundary migration. ODF examinations revealed that the texture components were almost the same as those developed in the particle-free processed specimen. However, the strength of rotated Cube texture component decreased while shear component C became stronger. In case of applying 3 volume percent of SiC nanoparticles, the stir zone grain size of 5.2 μm was obtained (Fig. 10). ODF analysis manifested the completion of development of shear texture component C from the rotated Cube. Of course, the overall texture strength became weaker due to the activation of particle stimulated nucleation (PSN) forming randomly oriented grains (compare Fig. 9 with Fig. 10).

4.3. Effect of cooling media

There are a large number of studies in the literature examining FSP under rapid cooling conditions to fabricate UFG aluminum alloys [66-68]. For example, Feng et al. [66] performed submerged FSP of 2219-T6 aluminum alloy in a room temperature water tank. They found that the grain size decreased from 17 μm in the base metal to around 1.3 μm in the stir zone (in case of rotational speed of 1000 rpm) with a small fraction in the range of 500-800 nm. When rotational speed decreased to 600 rpm, an average stir zone grain size of 0.8 μm could be achieved demonstrating the capability of FSP to produce UFG microstructure. Of course, in their study the base metal was not in the severely deformed condition. Khorrami et al. [69] examined the effect of cooling media on the stir zone microstructure of 1050-aluminum alloy preliminarily processed by 2 passes of CGP. To do so, the severely deformed specimen was processed by one pass of FSP under normal cooling condition and cryogenic temperature cooling medium. Microstructural assessments (Fig. 11 and Fig. 12) revealed that both cooling media resulted in the deterioration of subgrain structure developed in the severely deformed aluminum. The Zener-Hollomon (Z) parameter (Eq. (1)) reflecting the temperature (T) compensated strain

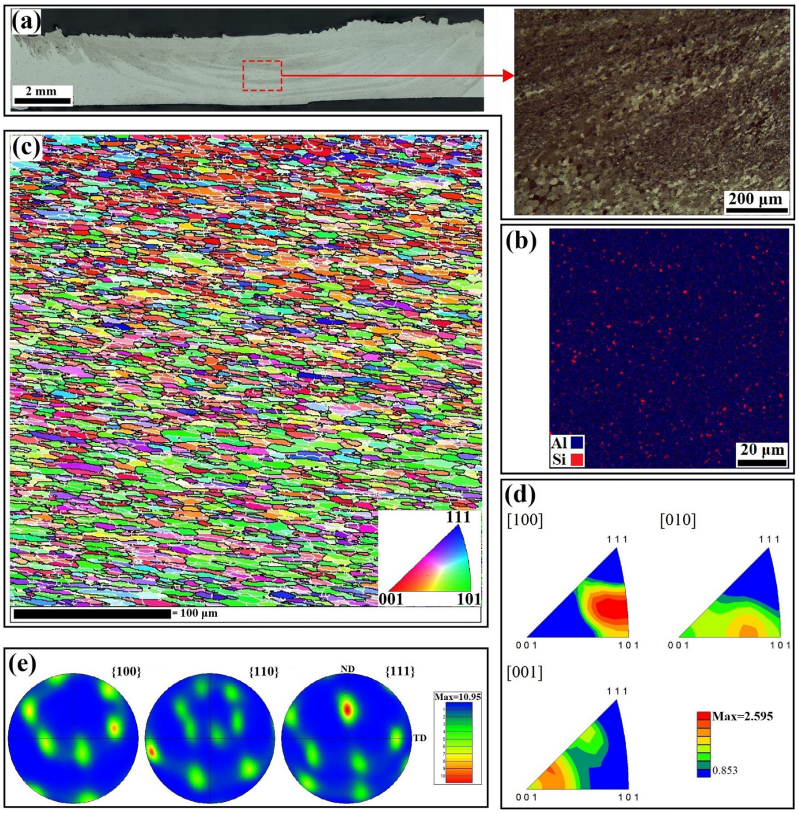

Fig. 10- Experimental results of 1050 aluminum alloy processed by 2 passes of CGP and subsequent 3 passes of FSP with 3 volume percent of SiC nanoparticles: (a) optical macro- and micrograph, (b) SEM elemental map showing distribution of nanoparticles, (c) EBSD grain orientation map, (d) inverse pole figures, and (e) pole figures from the stir zone[65].

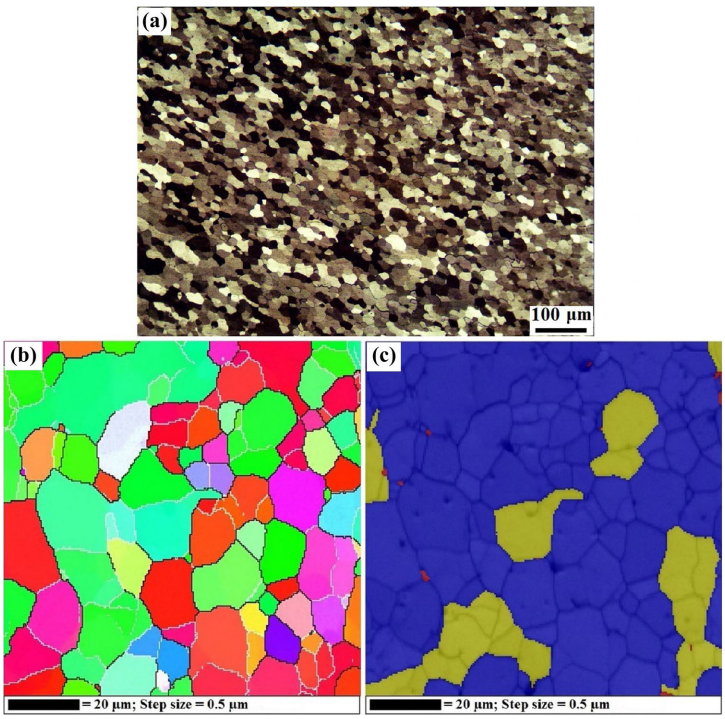

Fig. 11- Stir zone microstructure of the specimen processed under normal cooling condition: (a) optical microscopy image, (b) EBSD map, and (c) grain orientation spread (GOS) map; blue, red, and yellow grains denoted recrystallized, distorted, and substructured grains, respectively [69].

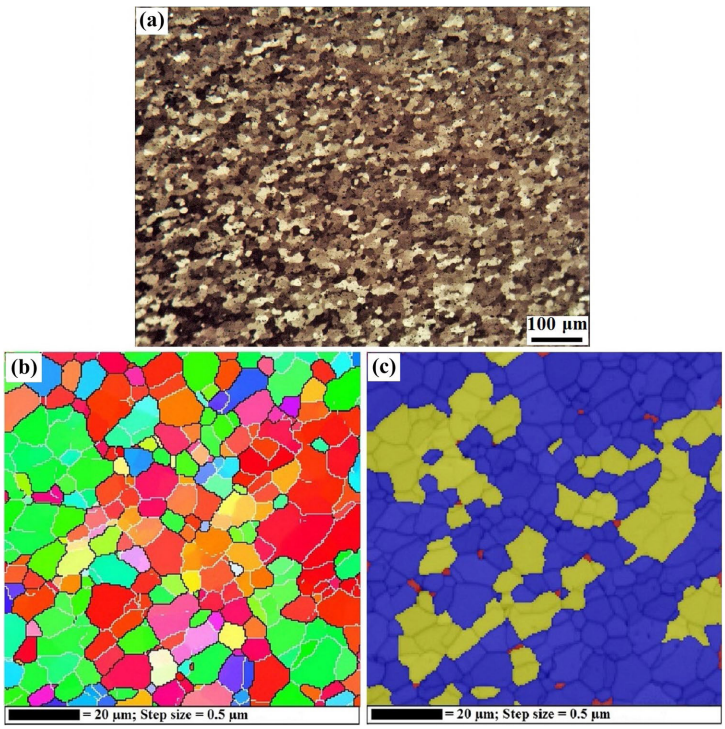

Fig. 12- Stir zone microstructure of the specimen processed under cryogenic cooling medium: (a) optical microscopy image, (b) EBSD map, and (c) GOS map; blue, red, and yellow grains denoted recrystallized, distorted, and substructured grains, respectively [69].

rate ($\dot{\varepsilon}$) determines the grain size of the stir zone:

$$Z = \dot{\varepsilon} \exp(-\frac{Q}{RT}) \quad (1)$$

where Q and R denote the activation energy for self-diffusion and gas constant, respectively. Processing under normal cooling condition led to the formation of equiaxed grains with average grain size of 13 μm and 60% of HAGBs. The obtained grain size is larger than that estimated by the Z parameter. This is attributed to large driving force for grain growth induced by the strain stored during SPD. However, processing under cryogenic cooling medium resulted in the formation of lower grain size in the stir zone as excessive grain growth was inhibited. In this case, the Z parameter could precisely predict the grain size of the stir zone.

This innovative method has positive effects not only in the stir zone but also in HAZ and TMAZ. Khorrami et al. [54] examined the microstructure and texture evolutions ahead of the FSP tool (Fig. 13) to realize the effect of cooling media on the FSP of UFG aluminum alloy. In this research a 1050 aluminum alloy was initially processed by 2 passes of CGP followed by FSP submerged in liquid Nitrogen. Optical microscopy and EBSD assessments revealed the occurrence of microstructure instability in the form of abnormal grain growth (AGG). They attributed it to combined effects associated with strong texture components and intense gradient in the stored strain of the severely deformed base metal. In fact the extremely high cooling rate during submerged FSP impeded the normal grain growth that is common during routine FSP (see Fig. 3 and ref [52]). Rather, the grains with orientations different from the dominant texture could involve in AGG and developed a Cube and Goss texture components. Steep gradients within the shear textured volume could provide conditions required by AGG. In this case, growth path is toward the areas with higher local misorientation, known as strain-induced grain boundary migration (SIGBM). Pole figure maps (Fig. 13 (c)) and ODF analysis (Fig. 14) from ahead of the FSP tool demonstrated that the stored strain of the base metal was not completely released and then the texture components of Brass, rotated Goss, and $B/\overline{B}$ (observed in the base metal) were partially preserved. Moreover, the abnormally grown grains were free from substructure (known as recrystallized grains) as well as internal misorientation as indicated in Fig. 15. More details regarding the effect of texture and stored strain on the AGG could be found in [70] and[71,72],

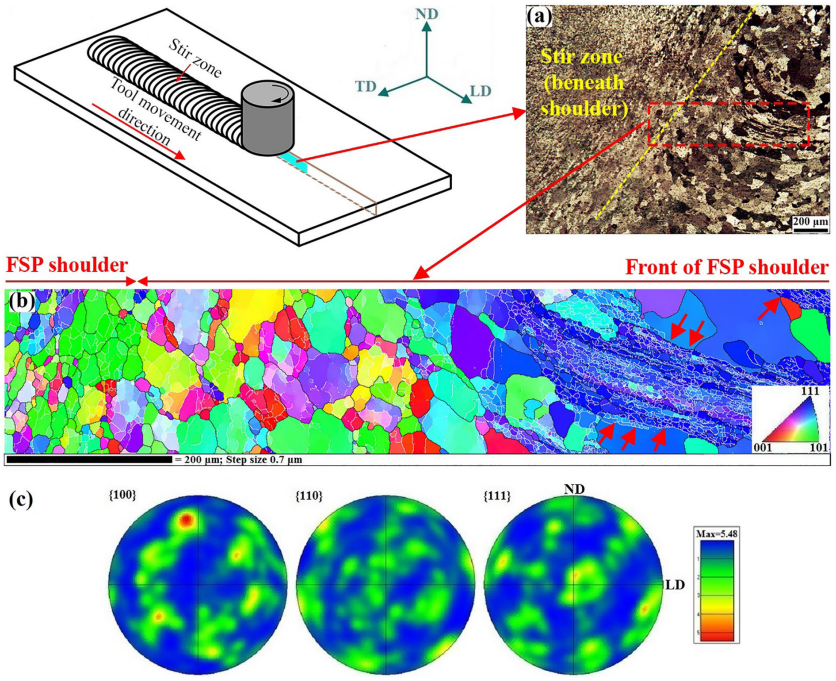

Fig. 13- Microstructure and texture evolutions ahead of the tool during cryogenic FSP of aluminum alloy processed by CGP: (a) Optical microscopy image, (b) EBSD map, and (c) pole figure maps [54].

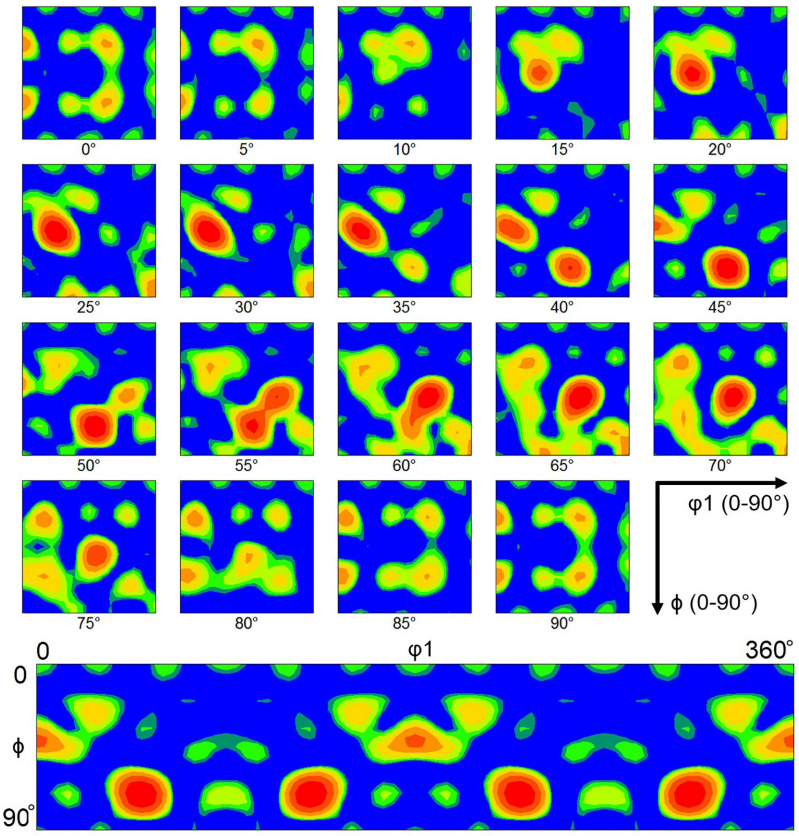

Fig. 14- ODF maps from ahead of the tool for 1050 Al alloy undergone submerged FSP after CGP: the Euler space angles of ϕ1=0−90° and φ=0−90° at ϕ2 sections in 5° intervals (top) and at the Euler space angles of ϕ1=0−360° and φ=0−90° at section ϕ2=0 (bottom) [54].

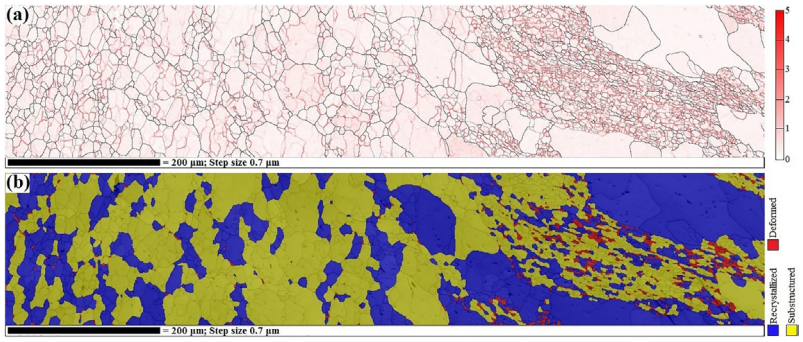

Fig. 15- (a) Local misorientation map and (b) GOS map from regions corresponding to Fig. 10 (b) [54].

respectively. A slight number of deformed grains (shown as "red" grains in GOS map) remained ahead of the tool, suggesting considerable amount of stored strain was released. However, elongated grains formed during CGP were still observed.

In order to have both positive effects associated with the addition of secondary nanoparticles and applying rapid cooling during FSP, it is possible to distribute reinforcing particles during submerged FSP that is carried out in [73]. In this study, SiC nanoparticles were dispersed in an UFG aluminum alloy through 3 passes of FSP submerged in the liquid Nitrogen. Fig. 16 shows the obtained stir zone microstructure signifying uniform dispersion of nanoparticles. Also, the EBSD and pole figure maps are indicated in Fig. 17. This innovative processing route resulted in the very fine grain structure in the stir zone. However, in comparison with the specimen processed under normal cooling condition, the texture strength became lower possibly due to

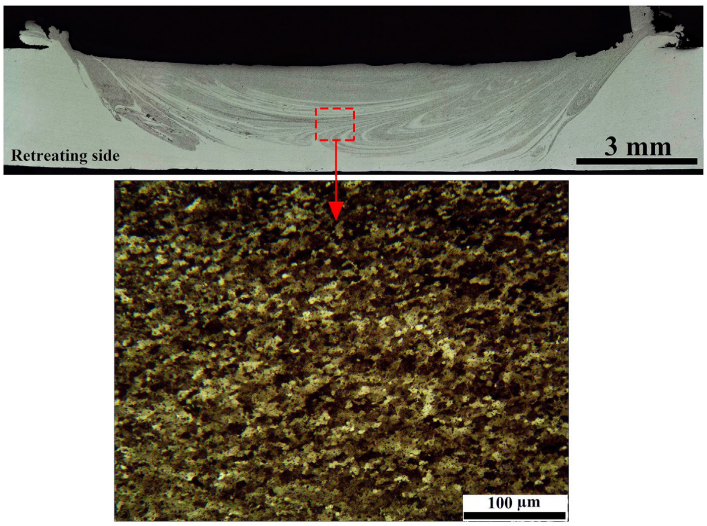

Fig. 16- Optical microscopy images showing the stir zone containing 1.5 volume percent of SiC nanoparticles obtained with FSP of UFG aluminum alloy under cryogenic cooling medium [73].

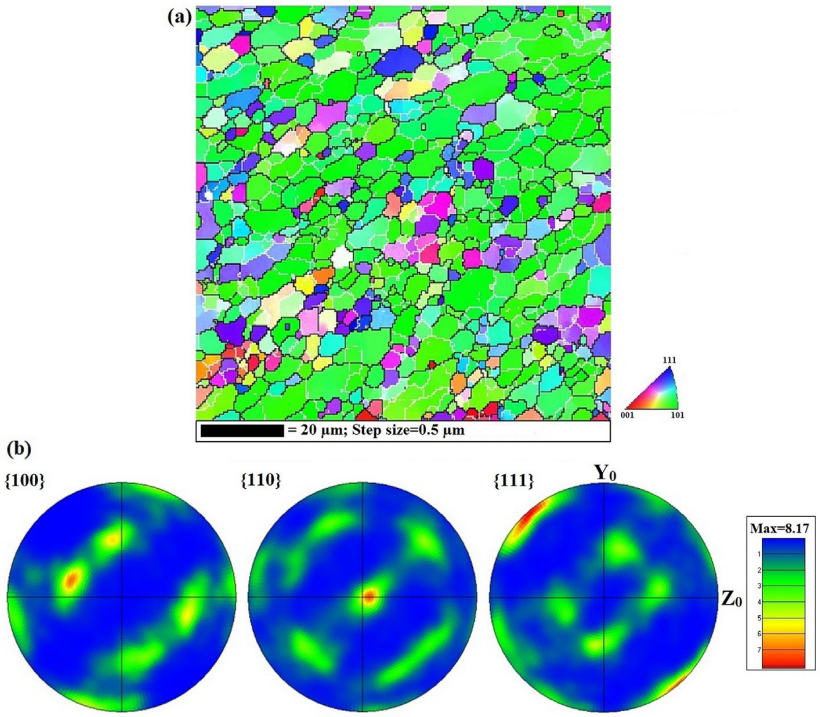

Fig. 17- EBSD results from stir zone of UFG aluminum alloy processed by FSP using 1.5 volume percent of SiC nanoparticles under cryogenic cooling medium [73].

the existence of grains with different orientations from those developed by shear deformation. TEM examination (Fig. 18) revealed the formation of a grain surrounded by HAGBs and the size of ~100 nm that was unlikely to exist prior to FSP. This suggested the activation of DDRX mechanism in spite of high stacking fault energy of aluminum alloy.

4.4. Mechanical behavior

4.4.1. Tensile properties

Nikulin et al. [74] examined the FSW of UFG Al-Cu-Mg-Ag alloy under various heat treatment conditions. The UFG microstructure with the average grain size of 0.6 µm was obtained with 8 passes of ECAP at 250 °C followed by hot rolling

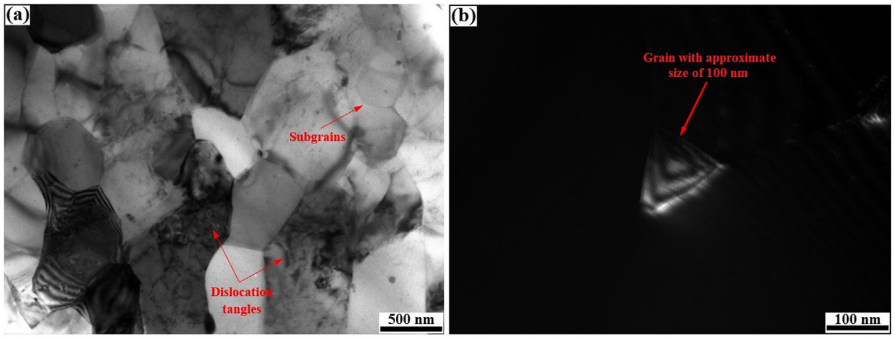

Fig. 18- TEM images in (a) bright field and (b) dark field modes from stir zone of UFG aluminum alloy processed by FSP using 1.5 volume percent of SiC nanoparticles under cryogenic cooling medium [73].

at 250 °C. The achieved plate was subsequently processed by FSW. Their results indicated that the grain size reached 2.3 μm in the stir zone implying the incident of grain growth during FSW. Tensile test was implemented to characterize mechanical properties of the alloy under various states (Fig. 19). As shown, the severely deformed specimen (denoted by SPD) exhibits continuous softening after limited work hardening. However, the welded specimen (SPD+FSW) has extensive uniform elongation, suggesting its high capacity of work hardening compared to the UFG base metal. The limited work hardening capacity of UFG materials is one of their common characteristics and is due to the high density of dislocation as well as localized plastic deformation from pre-existing shear bands formed during SPD [75]. As a result of work hardening effect, the weld showed higher ultimate strength (UTS) value than the UFG base metal. Rather, the yield strength (YS) of the base metal was more than that of the weld because of the grain size effect. The strength of UFG and welded materials increased after solution and artificial aging heat treatment (known as T6-temper). In this case, joint efficiencies of unity and of ~97% were reported for the YS and UTS, respectively. In spite of the deterioration of UFG microstructure after solution heat treatment at 520 °C, the strength of heat treated samples increased from 285 MPa to 405 MPa after aging in the light of dense precipitates that were uniformly dispersed [74].

Some researchers studied the mechanical properties of FSW joints of UFG aluminum alloys through transverse tensile test. For example, Khorrami et al. [76] examined mechanical properties of 1050 aluminum alloy subjected to FSW after CGP process. Their results had an indication of reduction in the strength after CGP process. Of course, the rate of decrease in the strength

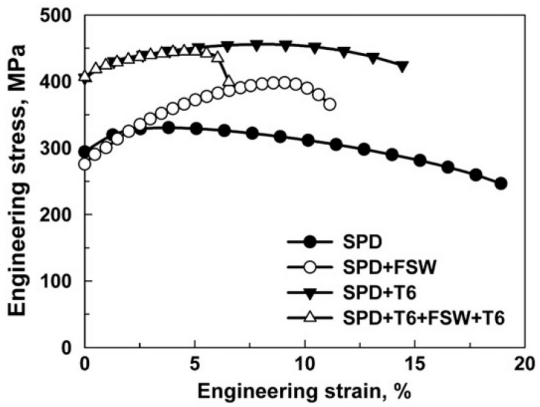

Fig. 19- Engineering stress-strain curves of Al-Cu-Mg-Ag alloy treated under various processing routes [74].

considerably depended on the initial stored strain value as well as welding parameters, i.e. welding rotational and traveling speeds. As shown in Fig. 20 (a), the FSW joint fractured from the interface of TMAZ and stir zone as a result of formation of elongated grains. The effect of rotation and traveling speeds on the strength of the FSW joints are illustrated in Fig. 20 (b) and (c), respectively. It is obvious that an increase in rotation speed of the FSW tool resulted in less tensile strength of the joints regardless of initial stored strain value (strain magnitude of 1.16 and 2.32 in specimens subjected to 1 and 2 passes of CGP process, respectively). Traveling speed had contrary effects on the tensile strength of the joints of specimens undergone 1 and 2 passes of CGP. The lower the traveling speed, the more the tensile strength in the joint of specimen processed by 1 pass of CGP. It has been attributed to the formation of more equiaxed grains at TMAZ as well as higher heat conduction while more elongated grains developed at TMAZ of specimen welded at higher traveling speed. For specimen processed by 2 passes of CGP process, microstructure instability

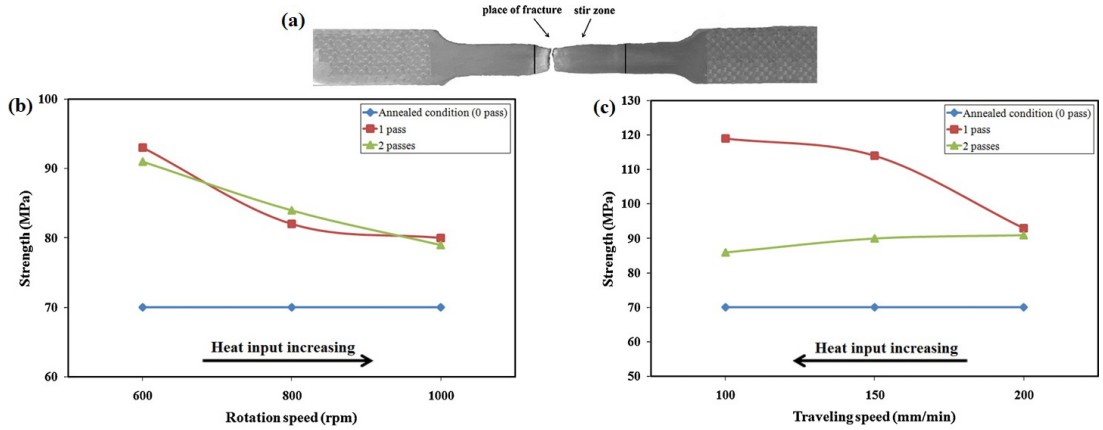

Fig. 20- (a) Place of fracture during transverse tensile test of 1050 aluminum alloy processed by CGP process followed by FSW, (b) and (c) shows the effect of rotation and traveling speeds on the strength of the FSW joints, respectively [76].

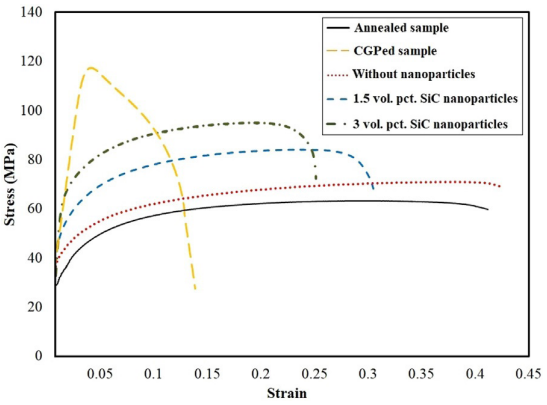

Fig. 21- Stress-strain curves of specimens prepared from 1050 aluminum alloy under annealed, severely deformed (CGPed), and friction stir processed using various amounts of secondary particles [65].

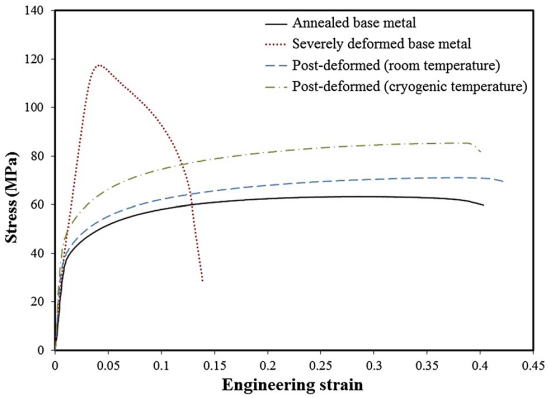

Fig. 22- Stress-strain curves obtained with tensile test of 1050 aluminum alloy under annealed, severely deformed, and post-deformed conditions [69].

dominantly occurred in all FSW conditions leading to appreciable reduction in tensile strength. Also, Fujii et al. [8] reported a considerable reduction in tensile strength of UFG 1050 aluminum alloy after FSW. Their joint specimens fractured from the stir zone during transverse tensile test.

In another research [65], the effect of volume fraction of secondary particles on the mechanical properties of the stir zone was examined. In this study, a 1050 aluminum alloy was severely deformed through 2 passes of CGP process followed by FSP using 0, 1.5, and 3 volume percent of SiC nanoparticles. Stress-strain curves from specimens extracted from the stir zone in the longitudinal direction are indicated in Fig. 21. It was observed that the application of FSP on the severely deformed aluminum alloy resulted in significant reduction in YS and UTS even when secondary nanoparticles were used. However, an increase in the volume fraction of nanoparticles enhanced both YS and UTS values at the expense of slight decrease in elongation magnitude. This also led to the increased work hardening rate that is common in specimens containing well dispersed secondary particles. Moreover, it was observed that fracture initiated from the interface of nanoparticles and the matrix. It was proposed that Orowan was the main strengthening mechanism in specimens containing nanoparticles while dislocation density governed the mechanical properties of particle-free specimens.

The effect of cooling media on the mechanical properties of UFG aluminum alloy processed by FSP was also investigated in [69]. In this research, severely deformed aluminum alloy specimens were post-deformed through FSP under room temperature and cryogenic cooling media (FSP submerged in liquid Nitrogen). Stress-strain curves obtained with tensile test from the stir zone are shown in Fig. 22.

Although cryogenic cooling media during FSP could effectively inhibit grain growth in the stir zone, considerable reductions in YS and UTS were observed in post-deformed specimens compared to the UFG base metal. The authors have attributed it to the deterioration of subgrain structure along with grain growth. However, the extent of strength drop was less in case of processing in the cryogenic cooling medium.

4.4.2. Hardness properties

Sun et al. [56] examined dissimilar FSW of UFG 1050 and 6061-T6 aluminum alloys. The microhardness profiles are shown in Fig. 23. As depicted, in the UFG side, a gradual decrease in the hardness value occurred as a result of grain growth and dislocation density drop. The same behavior was also observed in the 6061-T6 side due to the dissolution and, at the same time, coarsening of precipitates. Moreover, use of higher revolution pitch (corresponding to lower heat input) led to lower hardness drop in the HAZ. In the stir zone, the lowest hardness value was reported in the UFG side mainly due to the grain growth phenomenon. In another research study [6], FSW of UFG 1050 aluminum alloy processed by 5 cycles of ARB was examined. Also, the effect of H24 annealing of UFG alloy prior to FSW was studied. The related microhardness profiles are indicated in Fig. 24.

It was revealed that the stir zone hardness of as-received alloy increased compared to that of the base metal because of grain refinement caused by

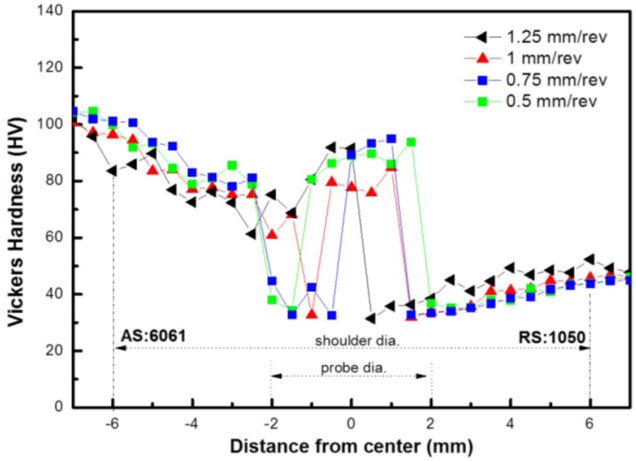

Fig. 23- Microhardness profiles across stir zone in UFG 1050 and 6061-T6 dissimilar FSW joints fabricated under various welding parameters [56].

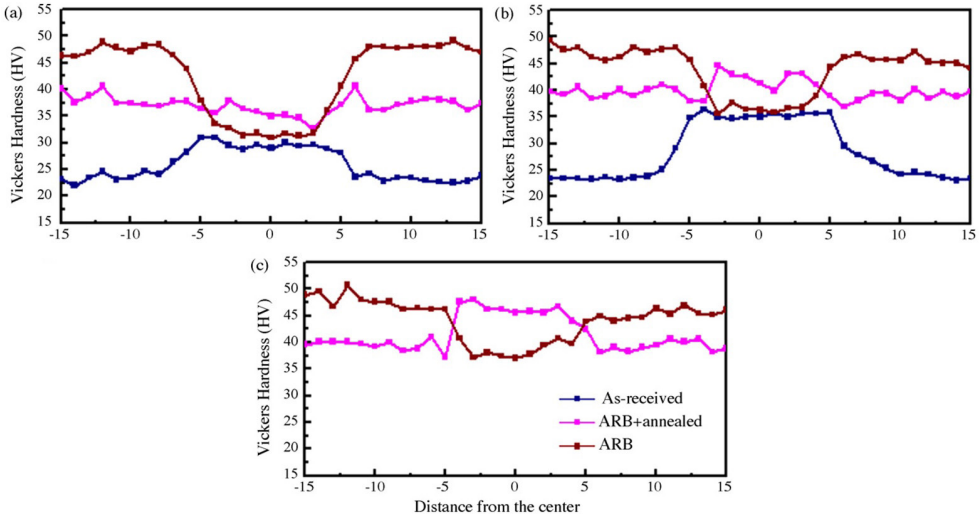

Fig. 24- Microhardness profiles across FSW joints of UFG 1050 aluminum processed under various revolution pitches of (a) 1.00, (b) 1.67, and (c) 2.50 mm/r [6].

DRX. However, the FSW resulted in a significant reduction in hardness value of the UFG alloy. It was in contrast to that observed in the UFG alloy undergone H24 annealing before FSW. The stir zone of this specimen exhibited the highest hardness values than those of as-received and UFG alloys. They attributed it to the instability of UFG alloy upon temperature rise during FSW while in the as-received and the UFG alloy undergone H24 annealing that had more stable microstructure, grain subdivision during FSW dominated rather than grain growth [6]. Sato et al. [12] published almost the same results on the FSW of UFG 1100 aluminum alloy. Based on the results obtained with the microhardness test (Fig. 25), they proposed that the strain stored in the base metal hardly affected microstructure of stir zone. This argument is contrary to that reported by other researches who

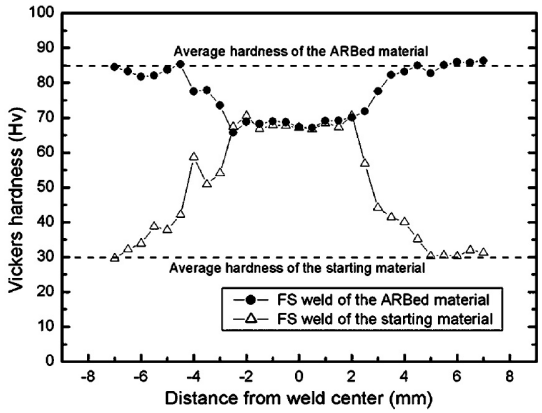

Fig. 25- Microhardness profiles across the stir zone of starting and UFG alloys after FSW under rotational and traveling speeds of 500 rpm and 12 mm/s, respectively [12].

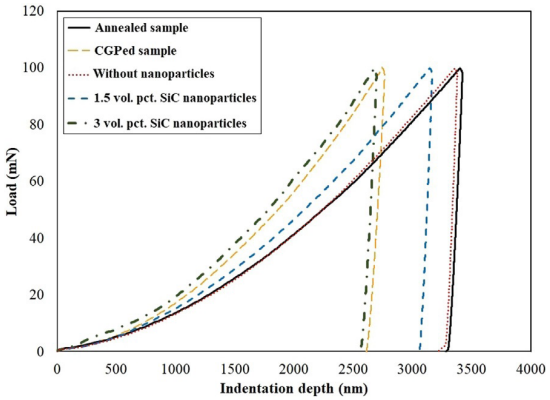

Fig. 26- Indentation curves for 1050 aluminum alloy under various conditions of fully annealed, severely deformed by CGP, and friction stir processed after CGP using 0, 1.5, and 3 volume percent of SiC nanoparticles [65].

emphasized that the stored strain could provide excessive driving force for grain growth after DRX during FSW [6,51]. As mentioned in the previous section, the addition of secondary nanoparticles during FSW/FSP of UFG aluminum alloys could effectively prevent growth of grains newly formed by DRX. In another research [65], the effect of applying SiC nanoparticles during FSP of 1050 aluminum alloy preliminarily severely deformed by CGP process. The related curves as well as quantitative results obtained with indentation test are indicated in Fig. 26 and Fig. 27, respectively. As can be seen, the application of CGP process caused a significant increase in the hardness value compared to the annealed specimen. This was related to the grain refinement along with increase in dislocation density after CGP process. The application of FSP without secondary particles led to an appreciable reduction in hardness value of the stir zone due to grain growth. However, the stir zone hardness increased with increasing the volume fraction of nanoparticles because of multilateral effects associated with their presence. They inhibited grain growth during FSP by pinning of grain boundaries. Additionally, the use of nanoparticles activated several strengthening mechanisms among which dislocation pinning, or Orowan mechanism, was more pronounced. The addition of SiC nanoparticles during FSP was also responsible for increased elastic modulus of the stir zone that is consistent with the rule of mixture.

5. Summary

UFG aluminum alloys consist of unstable grain boundaries that susceptible them to heating cycle. In this regard, the welding of these alloys

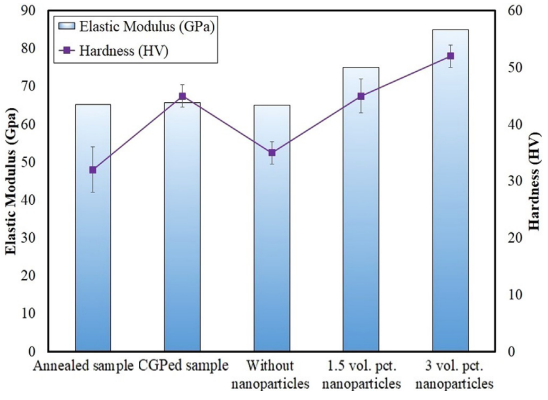

Fig. 27- Elastic modulus and hardness values obtained with indentation test of 1050 aluminum alloys under various conditions [65].

confronts with many challenges, specifically fusion state welding process is utilized. To overcome this difficulty, solid state welding process such as FSW seems to be suited for this purpose. The present review aims to outline the current state-of-the-art processing of UFG aluminum alloys by FSW/FSP. Particular issues, including microstructure and texture evolutions, effect of secondary particles and cooling media are discussed. Moreover, mechanical behaviors in terms of tensile properties and hardness measurements are reviewed. It is obvious that HAZ as well as the stir zone experiences considerable grain growth after FSW. DRV and DRX followed by grain growth completely deteriorate subgrain structure initially developed in the UFG alloy. More interestingly, static recrystallization and recovery occur in regions located ahead of the stir zone prior to being stirred by the rotating tool. This incident will affect the final microstructure of the stir zone. Shear texture components gradually developed ahead of the tool become stronger, suggesting GDRX mechanism is dominantly involved in the microstructure evolutions in the stir zone. The addition of secondary nanoparticles during FSP could restrict grain boundary migration and results in the formation of finer grain size and increased mechanical properties of the stir zone. This processing route does not change the main recrystallization mechanism but activates PSN which is responsible for the formation of randomly oriented grains and then reducing the overall texture strength. The accomplishment of FSP submerged in the cooling medium affects not only the microstructure of the stir zone but also that of regions around the rotating tool. Microstructure instability in the form of AGG induced by texture and stored strain. However, a finer grain size is obtained with this route. So, welding of UFG aluminum alloy could be successfully carried out by FSW if necessary measures, including the application of secondary particles and processing cooling medium are considered.

References

1. Valiev R. Nanostructuring of metals by severe plastic deformation for advanced properties. Nature Materials. 2004;3(8):511-6.
2. Sułkowski B, Janoska M, Boczkal G, Chulist R, Mroczkowski M, Pałka P. The effect of severe plastic deformation on the Mg properties after CEC deformation. Journal of Magnesium and Alloys. 2020;8(3):761-8.
3. Shin DH, Park J-J, Kim Y-S, Park K-T. Constrained groove pressing and its application to grain refinement of aluminum. Materials Science and Engineering: A. 2002;328(1-2):98-103.
4. Tsuji N, Saito Y, Utsunomiya H, Tanigawa S. Ultra-fine grained bulk steel produced by accumulative roll-bonding (ARB) process. Scripta Materialia. 1999;40(7):795-800.
5. Zangiabadi A, Kazeminezhad M. Development of a novel severe plastic deformation method for tubular materials: Tube Channel Pressing (TCP). Materials Science and Engineering: A. 2011;528(15):5066-72.
6. Sun Y, Fujii H, Takada Y, Tsuji N, Nakata K, Nogi K. Effect of initial grain size on the joint properties of friction stir welded aluminum. Materials Science and Engineering: A. 2009;527(1-2):317-21.
7. Ghosh M, Kumar K, Mishra RS. Analysis of microstructural evolution during friction stir welding of ultrahigh-strength steel. Scripta Materialia. 2010;63(8):851-4.
8. Fujii H, Cui L, Nakata K, Nogi K, Tsuji N, Ueji R. Mechanical properties of friction stir welds of ultrafine grained steel and other materials. InThe Fifteenth International Offshore and Polar Engineering Conference 2005 Jan 1. International Society of Offshore and Polar Engineers.
9. Sahin M, Erol Akata H, Ozel K. An experimental study on joining of severe plastic deformed aluminium materials with friction welding method. Materials & Design. 2008;29(1):265-74.
10. Topic I, Höppel HW, Göken M. Friction stir welding of accumulative roll-bonded commercial-purity aluminium AA1050 and aluminium alloy AA6016. Materials Science and Engineering: A. 2009;503(1-2):163-6.
11. Lilleby A, Grong Ø, Hemmer H. Cold pressure welding of severely plastically deformed aluminium by divergent extrusion. Materials Science and Engineering: A. 2010;527(6):1351-60.
12. Sato YS, Kurihara Y, Park SHC, Kokawa H, Tsuji N. Friction stir welding of ultrafine grained Al alloy 1100 produced by accumulative roll-bonding. Scripta Materialia. 2004;50(1):57-60.
13. Azushima A, Kopp R, Korhonen A, Yang DY, Micari F, Lahoti GD, et al. Severe plastic deformation (SPD) processes for metals. CIRP Annals. 2008;57(2):716-35.
14. Zrnik J, Dobatkin SV, Mamuzić I. Processing of metals by severe plastic deformation (SPD)–structure and mechanical properties respond. Metalurgija. 2008 Jul 1;47(3):211-6.
15. Valiev RZ, Islamgaliev RK, Alexandrov IV. Bulk nanostructured materials from severe plastic deformation. Progress in Materials Science. 2000;45(2):103-89.
16. Fatemi M, Zarei-Hanzaki A. Review on ultrafined/nanostructured magnesium alloys produced through severe plastic deformation: microstructures. Journal of Ultrafine Grained and Nanostructured Materials. 2015 Dec 1;48(2):69-83.
17. Mishra RS, Ma ZY. Friction stir welding and processing. Materials Science and Engineering: R: Reports. 2005;50(1-2):1-78.
18. Morawiński Ł, Chmielewski T, Olejnik L, Buffa G, Campanella D, Fratini L. Welding abilities of UFG metals. Author(s); 2018.
19. Gleiter H. Nanocrystalline materials. Progress in Materials Science. 1989;33(4):223-315.
20. Koch CC. Structural nanocrystalline materials: an overview. Journal of Materials Science. 2007;42(5):1403-14.
21. Valiev RZ, Estrin Y, Horita Z, Langdon TG, Zehetbauer MJ, Zhu Y. Producing Bulk Ultrafine-Grained Materials by Severe Plastic Deformation: Ten Years Later. JOM. 2016;68(4):1216-26.
22. Valiev RZ, Langdon TG. Principles of equal-channel angular pressing as a processing tool for grain refinement. Progress in Materials Science. 2006;51(7):881-981.
23. Mohammad Nejad Fard N, Mirzadeh H, Mohammad R, Cabrera JM. Accumulative roll bonding of aluminum/stainless steel sheets. Journal of Ultrafine Grained and Nanostructured Materials. 2017 Jun 1;50(1):1-5.
24. Todaka Y, Umemoto M, Yamazaki A, Sasaki J, Tsuchiya K.

Influence of High-Pressure Torsion Straining Conditions on Microstructure Evolution in Commercial Purity Aluminum. MATERIALS TRANSACTIONS. 2008;49(1):7-14.
25. Hadi S, Paydar MH. Investigation on the properties of high pressure torsion (HPT) processed Al/B4C composite. Journal of Ultrafine Grained and Nanostructured Materials. 2020 Dec 28;53(2):146-57.
26. Khajezade A, HABIBI PM, Mirzadeh H, MONTAZERI PM. Grain refinement efficiency of multi-axial incremental forging and shearing: A Crystal Plasticity Analysis.
27. Starink MJ, Qiao XG, Zhang J, Gao N. Predicting grain refinement by cold severe plastic deformation in alloys using volume averaged dislocation generation. Acta Materialia. 2009;57(19):5796-811.
28. Zhilyaev AP, Kim BK, Nurislamova GV, Baró MD, Szpunar JA, Langdon TG. Orientation imaging microscopy of ultrafine-grained nickel. Scripta Materialia. 2002;46(8):575-80.
29. Ghorbanpour M, Mazloumi M, Nouri A, Lotfiman S. Silver-doped nanoclay with antibacterial activity. Journal of Ultrafine Grained and Nanostructured Materials. 2017 Dec 1;50(2):124-31.
30. Huang H, Liu H, Wang C, Sun J, Bai J, Xue F, et al. Potential of multi-pass ECAP on improving the mechanical properties of a high-calcium-content Mg-Al-Ca-Mn alloy. Journal of Magnesium and Alloys. 2019;7(4):617-27.
31. Zrnik J, Kovarik T, Novy Z, Cieslar M. Ultrafine-grained structure development and deformation behavior of aluminium processed by constrained groove pressing. Materials Science and Engineering: A. 2009;503(1-2):126-9.
32. Colligan K. Material flow behavior during friction stir welding of aluminum. WELDING JOURNAL-NEW YORK-. 1999 Jul 1;78:229-s.
33. Morishige T, Hirata T, Tsujikawa M, Higashi K. Comprehensive analysis of minimum grain size in pure aluminum using friction stir processing. Materials Letters. 2010;64(17):1905-8.
34. Nasiri Z, Sarkari Khorrami M, Mirzadeh H, Emamy M. Enhanced mechanical properties of as-cast Mg-Al-Ca magnesium alloys by friction stir processing. Materials Letters. 2021;296:129880.
35. Bajakke PA, Jambagi SC, Malik VR, Deshpande AS. Friction Stir Processing: An Emerging Surface Engineering Technique. Surface Engineering of Modern Materials: Springer International Publishing; 2020. p. 1-31.
36. Fonda R. Development of grain structure during friction stir welding. Scripta Materialia. 2004;51(3):243-8.
37. Prangnell PB, Heason CP. Grain structure formation during friction stir welding observed by the 'stop action technique'. Acta Materialia. 2005;53(11):3179-92.
38. Ma ZY. Friction Stir Processing Technology: A Review. Metallurgical and Materials Transactions A. 2008;39(3):642-58.
39. Su J-Q, Nelson TW, Sterling CJ. Friction stir processing of large-area bulk UFG aluminum alloys. Scripta Materialia. 2005;52(2):135-40.
40. Su J-Q, Nelson TW, McNelley TR, Mishra RS. Development of nanocrystalline structure in Cu during friction stir processing (FSP). Materials Science and Engineering: A. 2011;528(16-17):5458-64.
41. Sarkari Khorrami M, Movahedi M. Microstructure evolutions and mechanical properties of tubular aluminum produced by friction stir back extrusion. Materials & Design (1980-2015). 2015;65:74-9.
42. Kwan C, Wang Z, Kang S-B. Mechanical behavior and microstructural evolution upon annealing of the accumulative roll-bonding (ARB) processed Al alloy 1100. Materials Science and Engineering: A. 2008;480(1-2):148-59.
43. Cao WQ, Godfrey A, Liu W, Liu Q. Annealing behavior of aluminium deformed by equal channel angular pressing. Materials Letters. 2003;57(24-25):3767-74.
44. Khorrami MS, Kazeminezhad M, Kokabi AH. Thermal stability of aluminum after friction stir processing with SiC nanoparticles. Materials & Design. 2015;80:41-50.
45. Sarkari Khorrami M, Kazeminezhad M, Kokabi AH. Thermal stability during annealing of friction stir welded aluminum sheet produced by constrained groove pressing. Materials & Design. 2013;45:222-7.
46. Sarkari Khorrami M, Kazeminezhad M, Kokabi AH. Microstructure evolutions after friction stir welding of severely deformed aluminum sheets. Materials & Design. 2012;40:364-72.
47. Su JQ, Nelson TW, Mishra R, Mahoney M. Microstructural investigation of friction stir welded 7050-T651 aluminium. Acta Materialia. 2003;51(3):713-29.
48. Su J-Q, Nelson TW, Sterling CJ. Microstructure evolution during FSW/FSP of high strength aluminum alloys. Materials Science and Engineering: A. 2005;405(1-2):277-86.
49. Jata KV, Semiatin SL. Continuous dynamic recrystallization during friction stir welding of high strength aluminum alloys. Scripta Materialia. 2000;43(8):743-9.
50. Kumar N, Mishra RS, Huskamp CS, Sankaran KK. Microstructure and mechanical behavior of friction stir processed ultrafine grained Al–Mg–Sc alloy. Materials Science and Engineering: A. 2011;528(18):5883-7.
51. Khorrami MS, Kazeminezhad M, Kokabi AH. Influence of Stored Strain on Fabricating of Al/SiC Nanocomposite by Friction Stir Processing. Metallurgical and Materials Transactions A. 2015;46(5):2021-34.
52. Sarkari Khorrami M, Kazeminezhad M, Miyashita Y, Kokabi AH. The Correlation of Stir Zone Texture Development with Base Metal Texture and Tool-Induced Deformation in Friction Stir Processing of Severely Deformed Aluminum. Metallurgical and Materials Transactions A. 2016;48(1):188-97.
53. Naseri M, Reihanian M, Borhani E. EBSD characterization of nano/ultrafine structured Al/Brass composite produced by severe plastic deformation. Journal of Ultrafine Grained and Nanostructured Materials. 2018 Dec 1;51(2):123-38.
54. Sarkari Khorrami M, Saito N, Miyashita Y. Texture and strain-induced abnormal grain growth in cryogenic friction stir processing of severely deformed aluminum alloy. Materials Characterization. 2019;151:378-89.
55. Emami S, Saeid T, Khosroshahi RA. Microstructural evolution of friction stir welded SAF 2205 duplex stainless steel. Journal of Alloys and Compounds. 2018;739:678-89.
56. Sun Y, Tsuji N, Fujii H. Microstructure and Mechanical Properties of Dissimilar Friction Stir Welding between Ultrafine Grained 1050 and 6061-T6 Aluminum Alloys. Metals. 2016;6(10):249.
57. Khorrami MS, Kazeminezhad M, Miyashita Y, Kokabi AH. Improvement in the mechanical properties of Al/SiC nanocomposites fabricated by severe plastic deformation and friction stir processing. International Journal of Minerals, Metallurgy, and Materials. 2017;24(3):297-308.
58. Sarkari Khorrami M, Kazeminezhad M, Kokabi AH. The effect of SiC nanoparticles on the friction stir processing of severely deformed aluminum. Materials Science and Engineering: A. 2014;602:110-8.
59. Ke L, Huang C, Xing L, Huang K. Al–Ni intermetallic composites produced in situ by friction stir processing. Journal of Alloys and Compounds. 2010;503(2):494-9.
60. Hsu CJ, Chang CY, Kao PW, Ho NJ, Chang CP. Al–Al3Ti nanocomposites produced in situ by friction stir processing. Acta Materialia. 2006;54(19):5241-9.

61. Bauri R, Yadav D, Suhas G. Effect of friction stir processing (FSP) on microstructure and properties of Al–TiC in situ composite. Materials Science and Engineering: A. 2011;528(13-14):4732-9.
62. Mishra RS, Ma ZY, Charit I. Friction stir processing: a novel technique for fabrication of surface composite. Materials Science and Engineering: A. 2003;341(1-2):307-10.
63. Soleymani S, Abdollah-zadeh A, Alidokht SA. Microstructural and tribological properties of Al5083 based surface hybrid composite produced by friction stir processing. Wear. 2012;278-279:41-7.
64. Padmanaban G, Balasubramanian V. Selection of FSW tool pin profile, shoulder diameter and material for joining AZ31B magnesium alloy – An experimental approach. Materials & Design. 2009;30(7):2647-56.
65. Sarkari Khorrami M, Saito N, Miyashita Y, Kondo M. Texture variations and mechanical properties of aluminum during severe plastic deformation and friction stir processing with SiC nanoparticles. Materials Science and Engineering: A. 2019;744:349-64.
66. Feng X, Liu H, Lippold JC. Microstructure characterization of the stir zone of submerged friction stir processed aluminum alloy 2219. Materials Characterization. 2013;82:97-102.
67. Liu HJ, Feng XL. Effect of post-processing heat treatment on microstructure and microhardness of water-submerged friction stir processed 2219-T6 aluminum alloy. Materials & Design. 2013;47:101-5.
68. Rui-dong F, Zeng-qiang S, Rui-cheng S, Ying L, Hui-jie L, Lei L. Improvement of weld temperature distribution and mechanical properties of 7050 aluminum alloy butt joints by submerged friction stir welding. Materials & Design. 2011;32(10):4825-31.
69. Khorrami MS, Kazeminezhad M. Post Deformation at Room and Cryogenic Temperature Cooling Media on Severely Deformed 1050-Aluminum. Metals and Materials International. 2018;24(2):401-14.
70. Humphreys FJ, Hatherly M. Recrystallization and related annealing phenomena. Elsevier; 2012 Dec 2.
71. Zhang J-m, Xu K-w, Ji V. Strain-energy-driven abnormal grain growth in copper films on silicon substrates. Journal of Crystal Growth. 2001;226(1):168-74.
72. Bozzolo N, Agnoli A, Souaï N, Bernacki M, Logé RE. Strain Induced Abnormal Grain Growth in Nickel Base Superalloys. Materials Science Forum. 2013;753:321-4.
73. Khorrami MS, Kazeminezhad M, Miyashita Y, Saito N, Kokabi AH. Influence of ambient and cryogenic temperature on friction stir processing of severely deformed aluminum with SiC nanoparticles. Journal of Alloys and Compounds. 2017;718:361-72.
74. Nikulin I, Malopheyev S, Kipelova A, Kaibyshev R. Effect of SPD and friction stir welding on microstructure and mechanical properties of Al–Cu–Mg–Ag sheets. Materials Letters. 2012;66(1):311-3.
75. Satheesh Kumar SS, Raghu T. Strain path effects on microstructural evolution and mechanical behaviour of constrained groove pressed aluminium sheets. Materials & Design. 2015;88:799-809.
76. Khorrami MS, Kazeminezhad M, Kokabi AH. Mechanical properties of severely plastic deformed aluminum sheets joined by friction stir welding. Materials Science and Engineering: A. 2012;543:243-8.